ORIGINAL PAPER

Performance of Genetic Programming and Multivariate Adaptive Regression Spline Models to Predict Vibration Response of Geocell Reinforced Soil Bed: A Comparative Study

Hasthi Venkateswarlu[1] · Shivpreet Sharma[1] · A. Hegde[1]

Abstract

This paper explores the applicability of rapidly growing machine learning techniques (MLTs) for predicting the vibration response of geocell reinforced soil beds. Peak particle velocity (PPV) is used as an indicator to represent the vibration response. Two machine learning techniques namely, Genetic programming (GP), and multivariate adaptive regression splines (MARS) are used for the PPV prediction. Primarily, a series of field vibration tests were conducted over the geocell reinforced beds to obtain the dataset for model development. During the field test, PPV variation was studied by varying the test parameters namely, footing embedment, dynamic load, modulus of infill material, width, and depth of placement of geocell mattress. In total, 240 field measurements were used to formulate the PPV prediction models. The prediction performance of a developed model was examined by determining the different statistical indices. In addition, the ranking of each input parameter was calculated to identify the parameter, which influences the PPV most. According to the outcome of developed models, coefficient of determination (R^2) values of (0.9918, 0.9852), and (0.9949, 0.9941), were observed for training and testing data sets of GP and MARS models, respectively. The sensitivity analysis of both the models revealed that the distance from the source to the measurement point indicating the damping properties of the reinforced bed is predominantly affecting PPV. Further, a comparative study has been carried out to examine the efficiency of the developed model in predicting the PPV response at the unknown dynamic excitation. The results of the comparative analysis revealed that the MARS model exhibits a high degree of accuracy in predicting the PPV variation in comparison to GP.

Keywords Peak particle velocity · Geocell · Field vibration test · Genetic programming · Multivariate adaptive regression splines

Introduction

Controlling the detrimental effects that result from the intense levels of ground vibration has received substantial attention in the recent past. Earthquakes, high-speed train systems, mine explosions, nuclear power plants, pile driving, dynamic compaction, and vibrating machines are the practical sources of vibration. Risk levels of induced vibration are typically expressed using the parameter, peak particle velocity (PPV). It represents the maximum velocity attained by the soil particle due to the induced vibration in each of the three mutually orthogonal directions. It is also used to represent the level of risk experienced by the structures located near the vibration source. Presently, different standards provide different PPV limits for monitoring the life of old structures or monuments. A summary of threshold PPV limits suggested by different standards is provided in Table 1.

To mitigate the vibration effect, one of the strategies is to enhance the elastic response of the foundation bed. Reinforced earth using geosynthetics is one of the most efficient approaches to serve this purpose. Among the different geosynthetics, geocell found to exhibit superior performance over the other forms of geosynthetics for reinforcement

✉ Hasthi Venkateswarlu
hasthi.pce16@iitp.ac.in

Shivpreet Sharma
shivpreetshrm@gmail.com

A. Hegde
ahegde@iitp.ac.in

1   Department of Civil and Environmental Engineering, Indian Institute of Technology Patna, Bihta 801106, Bihar, India

Table 1 Threshold values of vibration limits based on different standards

Standard		Excitation frequency in Hz	Peak particle velocity (mm/s)		
			Structures of historic/ sensitive importance	Domestic buildings	Industrial buildings
AASHTO [1]		NR	2.5	5.1	25.4
BS 7385-2 [2]		15–40	NR	20–50	NR
		>4	NR	NR	50
CMRI standard [3]		<24	2	5	12.5
		>24	5	10	25.5
DIN 4150-3 [4]		<10	3	5	20
		10–50	3–8	5–15	20–40
		50–100	8–10	15–20	40–50
DGMS India [5]	Buildings belonging to owners	<8	2	5	10
		8–25	5	10	20
		>25	8	15	25
	Buildings not belonging to owners	<8	NR	10	15
		8–25	NR	15	25
		>25	NR	20	50
SN 640-312 [6]		<10	NR	12.7	NR
		10–60	7.6	13.7	30.5
		60–90	7.6–12.7	12.7–17.8	30.5–40.6
USBM RI 8507 [7]		10–40	NR	15.7–50.8	NR
		4–15	NR	15–20	NR
USSR [8]		NR	8	30	60

NR not reported

application [9, 10]. Further, the strengthening aspect of geocell has been widely recognized in improving the stiffness of a foundation bed [11]. These are the important requirements for the safe performance of foundations subjected to vibration loads. Limited studies highlighted the potential benefits of geocell in minimizing the harmful effects of vibration. Venkateswarlu et al. [12] emphasized the ability of geocell in controlling the velocity of induced vibration through experimental investigation. Ujjawal et al. [13] developed a 3D numerical model to compute the isolation efficacy of geocell reinforced beds.

It is also an intriguing fact that only a few empirical methods are available to estimate the PPV caused by blast-induced vibration. These methods are not suitable to use for the prediction of PPV response induced by continuous type vibration sources such as industrial machines and transit systems. Under such circumstances, developing a scientific model for predicting the PPV response is very essential. In recent times, the application of machine learning techniques (MLTs) has grown rapidly for developing robust prediction models in the field of geotechnical engineering [14–18]. A few popular techniques include artificial neural networks (ANN), genetic programming (GP), fuzzy logic systems (FLS), support vector machine (SVM), and multivariate adaptive regression analysis

(MARS). The efficacy of few MLTs has also been highlighted in predicting the behavior of geosynthetics reinforced soil beds [19–22].

Raja and Shukla [23] reported that the MLTs are capable of developing the complex nonlinear relationship between the independent and dependent parameters. Several studies have employed the MLTs for predicting the PPV caused by blast-induced vibration [24–28]. These studies reveal that artificial neural networks (ANNs) and adaptive neuro-fuzzy inference systems (ANFIS) are preferred techniques for this purpose. Generally, the above methods are considered as block-box tools. Besides, the other difficulties of implementing such methods include the time-consuming process of developing the optimum network and local minima. To overcome these issues and to achieve a better prediction performance of non-linear response, other techniques namely, GP and MARS were developed [29–32]. The effectiveness of these methods has been prominently reported in assessing the stability of slopes, load-carrying capacity of piles, soil liquefaction, settlement of shallow foundations, and bearing capacity of strip footing, etc. [33–39]. Few studies reported the use of MARS in estimating the PPV due to blast loading stipulations [40, 41]. Importantly, the additional advantages of these methods include the ability to work with noisy data, easy interpretation, and more efficiency.

It is evident from the literature that, there is a lack of a simplified solution to determine the PPV response caused by the vibration source resting on the geocell reinforced foundation bed. In the present investigation, GP and MARS models are used to develop the PPV prediction equation for the scenario of geocell-reinforced bed supporting the vibration source, which can induce harmonic excitation. Prominently, this study is the first of its kind in developing, assessing, and comparing GP and MARS models in an attempt for predicting the PPV response of geocell reinforced bed supporting the vibration source. Initially, field vibration tests were performed over the geocell reinforced bed to develop the database. Using a field test database, PPV prediction models were established. Further, the best PPV prediction model is assessed by comparing the predictive performance of both the models against the unknown dataset obtained through the additional field vibration tests.

Machine Learning techniques

Methodology of Genetic Programming (GP)

Genetic Programming (GP) is the biologically supervised computing approach introduced by Koza [42]. This technique extends genetic algorithms (GAs) to evolve computer programs based on the principles of natural selection and genetics. Though the operation of GP and GAs are similar, the way of representation of a final solution is different in both techniques. The result of GP is generally expressed in the form of a tree structure [43]. Whereas, the result generated from GAs is expressed in the form of a string number.

The working architecture of the GP algorithm is shown schematically in Fig. 1. Initially, the pool of numerous potential solutions called a population is generated from the input database. The population consists of a random number of individuals. Symbolic representation of each individual is shown in Fig. 2a. It is comprised of a set of terminals and functions. Trigonometric functions, user-defined functions, Boolean, logical, and mathematical operators are the group of a functional set. Variables and numerical or logical constants are part of a terminal set.

The GP tree begins with a root node and prolongs up to the designated functional or terminal set. After generating the population of expressions, the ability of every individual expression to solve the problem is assessed using a fitness function. This process is continued until the termination criterion is fulfilled. Root mean square error (RMSE) was evaluated to fulfill the termination check. The foremost purpose of this practice is to minimize the error produced by the model. If the criteria are not fulfilled, a new population is generated based on different genetic operations namely, crossover, mutation, and reproduction. One can refer to
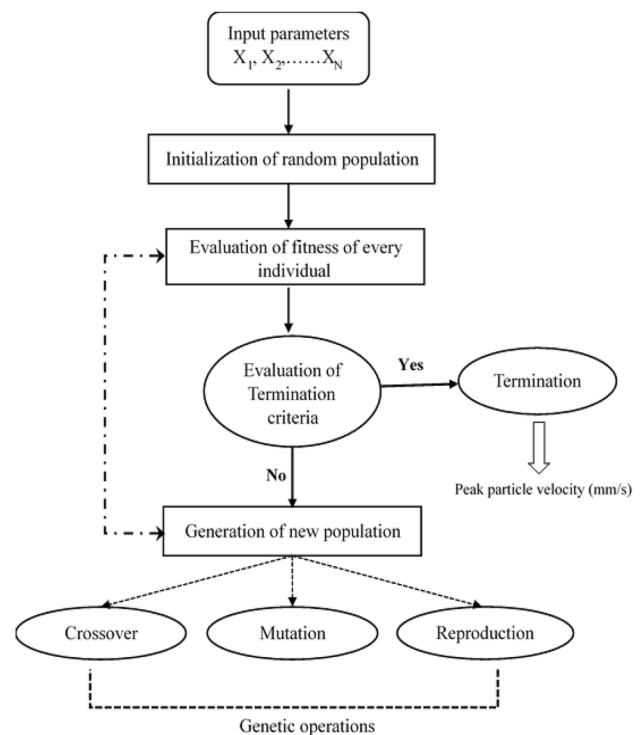

Fig. 1 Methodological architecture of GP

Koza [42] for more details about the initialization techniques. Finally, the best program obtained from the population through the termination check is considered as a PPV prediction model.

Further, Multi-Gene Genetic Programming (MGGP) is the other class of GP, which is used to establish the functional relationship between the input and output parameters [44, 45]. The mathematical expression is a result of the weighted linear combination of outputs. The schematic view of a typical multi-gene model adopted for predicting the output is shown in Fig. 2b. From the figure, the input parameters involved in the model are a_1, a_2, and a_3. Similarly, $\cos, \times, -,$ and $+$ are the functional parameters.

Methodology of MARS (Multivariate Adaptive Regression Splines)

The methodological architecture of a MARS model is shown schematically in Fig. 3. MARS is a statistical non-parametric regression method aids to predict nonlinear responses between dependent and independent variables using numerous splines of varying gradients. This method does not follow a specific assumption to develop the required relation using input indices. The end portion of each spline (linear segment) is referred to as a knot. It indicates the completion of one group of data and the beginning of another. The resulting segmental splines enrich the flexibility of a model
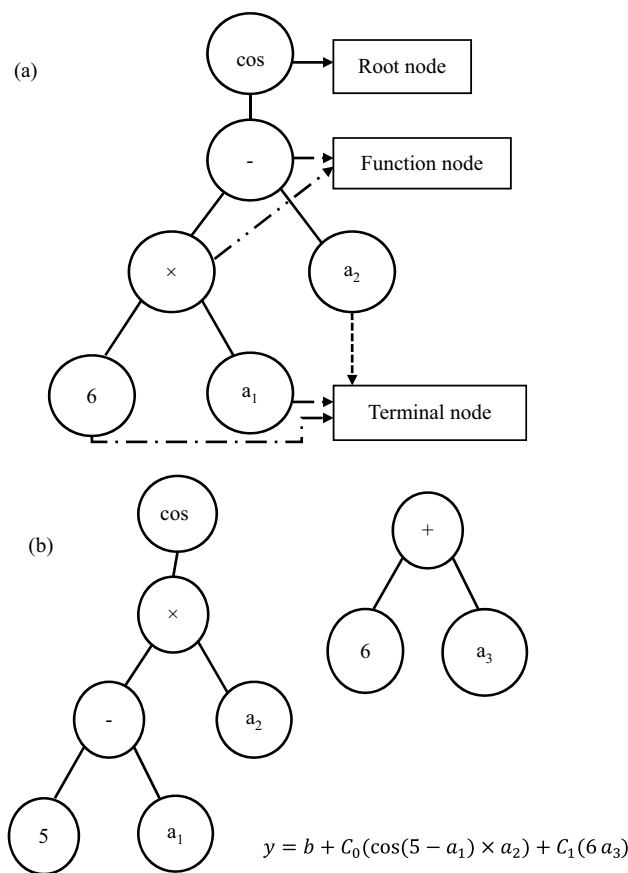
(a)

(b)

$$y = b + C_0(\cos(5 - a_1) \times a_2) + C_1(6\,a_3)$$

Fig. 2 Schematic view of genetic models: **a** randomly generated GP tree with the expression of cos ($6a_1 - a_2$); and **b** Multi-gene model

and allow the model to bend at any departure from the linear path. These segments are referred to as basis functions (BFs). Basis functions are generally categorized into two types, namely, linear piecewise and cubic piecewise. For simplicity, the piecewise linear function was used in the present study [46].

In this method, linear functions are expressed as max (0, $x-t$), where t is the location of the knot. The term max (.) signifies the consideration of positive value during the generation of BFs as reported below.

$$\max(0, x - t) = \begin{cases} x - t, & \text{if } x \geq t \\ 0, & otherwise \end{cases} \tag{1}$$

Generally, the MARS approach follows a two-step procedure to develop the optimum model. It includes a forward and backward iterative process. During the forward iterative stage, the model is formulated through the stepwise addition of BFs. In addition, a suitable location of knots is formed to enhance the model performance. During this stage, BFs cover a complete domain of the database to select the optimal pairs of spline functions by performing two-by-two

combinations. To develop the final model, all the BFs are combined as a weighted sum using the following expression.

$$Y(i) = \alpha_0 + \sum_{p=1}^{M} \alpha_p \emptyset_p(x) \tag{2}$$

where $Y(i)$ is the predicted value, α_0 is the constant coefficient of the basis function, $\emptyset_p(x)$ is the pth basis function, which may be a single spline or the combination of two spline functions, α_p is the numerical coefficient of pth BF, and M is the total number of BFs considered in the model.

In the backward iterative phase, the generated model is simplified by deleting the less important basis functions. This process is continued until the best set of basis functions are obtained. To prune the least contributed BFs, the MARS model follows the generalized cross-validation (GCV) criterion. The importance of a variable can be quantified by observing the variation in measured GCV in the absence of a particular variable from the model. This approach is beneficial for reducing the excessive number of spline functions and avoiding the chances of overfitting. GCV signifies the mean squared residual error divided by a penalty to account for the variance associated with model complexity [47].

Dataset Collection

Retrieving the sufficient database is the foremost aspect for the development of a prediction model. To do so, a series of field vibration tests were conducted over the geocell reinforced foundation beds. The details of field experiments performed for data collection are concisely discussed in the following section.

Details of Field Vibration Test

In total, 50 numbers of field vibration tests were performed over the geocell reinforced soil beds with varying configurations of load, geocell geometry, and footing embedment. The schematic sketch of the field vibration test is shown in Fig. 4. Test bed was prepared in the excavated pit of 3600 mm length, 3600 mm width, and 1200 mm height. The width and depth of the reinforced foundation bed were considered as 6B and 2B (B is the width of a concrete block), respectively, to minimize the boundary effect on the experimental results [13, 48]. To prepare the compacted bed, silty sand (SM) was used. The geocell made up of novel polymeric alloy (NPA) was used as a reinforcement. In addition to the silty sand, different materials namely, aggregate, construction and demolition waste (CDW), steel slag, and sand were used to fill the geocell pockets. These materials were classified as GP, GW, SW, SP, and SM respectively, based on the Unified Soil Classification System. The geotechnical properties of

Fig. 3 Methodological architecture of MARS

Peak particle velocity (mm/s)
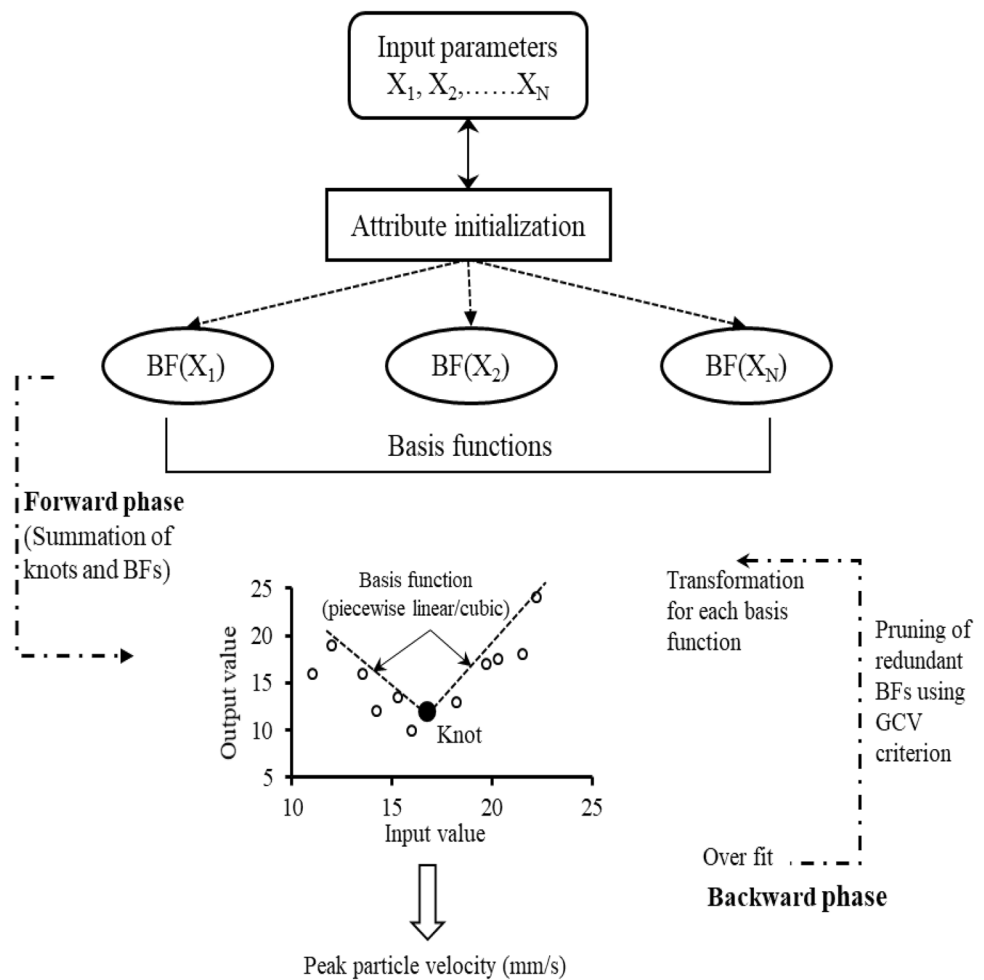
all the geo-materials are listed in Table 2. Elastic modulus (E) of infill materials was determined by performing the consolidated undrained triaxial test. Similarly, different geocell properties are listed in Table 3. Further, the detailed procedure of preparing the geocell reinforced bed has been reported by Venkateswarlu and Hegde [48].

After preparing the reinforced bed, the assembly of concrete block and oscillator was used to generate the vibration similar to a rotary machine. Dynamic force emanated by the oscillator relies on operating frequency and eccentric angle. During the test, the eccentricity controller was used for varying the eccentric angle (θ). A detailed description of θ and the estimation of dynamic force has been provided by Venkateswarlu et al. [4] elsewhere. To run the oscillator at varying operating frequencies, it was connected to a 6HP capacity DC motor with the flexible shaft assembly. The operating frequency was controlled using a speed control device (SCD). Accelerometers were used to measure the peak particle velocity (PPV) of soil particles at the applied dynamic force. It can monitor the PPV corresponding to three orthogonal directions. The resolution and maximum measuring range of the accelerometer were 0.01 mm/s and 200 mm/s, respectively. Total, 10 numbers of accelerometers were placed on the ground surface at an interval of 0.5 m from the face of the concrete block. Further, PPV was also measured at selected locations using 3D geophones to assess the accuracy of accelerometer recordings.

Total, four different series of experiments were conducted over the geocell reinforced bed to understand the PPV variation. It includes series I: vibration tests on geocell reinforced bed with varying geocell width (b) from 3 to $6B$ with an increment of $1B$ (B is the width of a concrete block). In series II, the depth of placement of geocell (U) was varied from $0.1B$ to $0.5B$ in the range of $0.2B$. The geocell reinforcement was infilled with different geomaterials in Series III. Similarly, the footing embedment was varied from $0B$ to $0.5B$ with an increment of $0.25B$ in the series IV. In each case, the variation of PPV was examined at two different dynamic force (F_d) levels i.e., 1 kN and 1.5 kN. A fresh reinforced test bed was prepared for each new test.
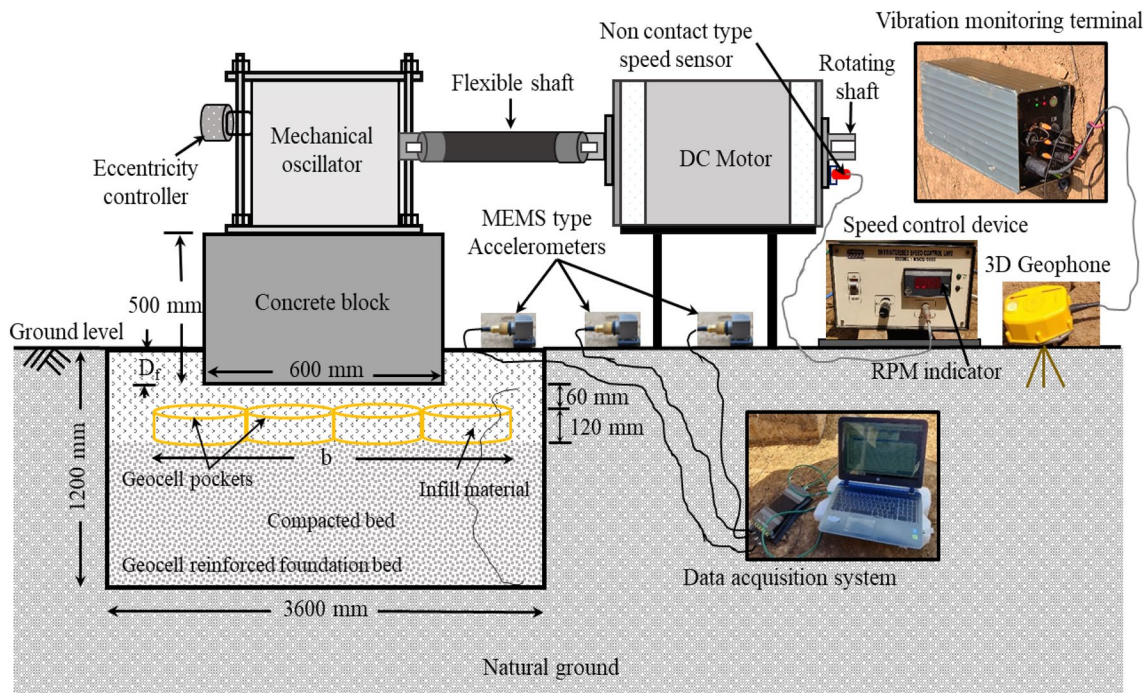
Fig. 4 Schematic outlook of field vibration test with ground conditions

Table 2 Properties of geo-materials

Geo-material	Parameter						
	D_{50} (mm)	C_u	C_c	d_{max}(kN/m³)[a]	d_{min} (kN/m³)[b]	E_g (MN/m²)[c]	φ (°)[d]
Aggregate	10.7	1.07	1.03	17.5	15.3	60	49
CDW	9.3	47.33	4.54	19.3	15.8	43	43
Steel slag	0.6	6.58	1.08	18.9	17.2	39	39
Sand	0.45	2.63	1.28	18.6	16.5	32	36
Silty sand	0.38	22.22	10.12	17.9	14.5	28.3	32

D_{50} is the average diameter; C_u is the uniformity coefficient; C_c is the coefficient of curvature; $_{dmax}$ is the maximum dry unit weight; $_{dmin}$ is the minimum dry unit weight; and E_g is the elastic modulus of geo-material

[a] ASTM D-4253 [49]

[b] ASTM D-4254 [50]

[c] ASTM D-4767 [51]

[d] ASTM D-3080 [52]

Experimental Results

PPV variation of geocell reinforced bed with respect to geocell width, depth of placement, type of infill, and footing embedment is presented in Fig. 5a–d. Figure 5a shows the influence of the width of the geocell mattress on the PPV. The rate of reduction of PPV was found to increase with the increase in width of the geocell. The decreasing trend of PPV represents the potential of geocell in obstructing the motion of induced vibration. PPV reduction rate became marginal beyond the geocell width of 5B (B is the width of

a concrete block). Thus, the geocell width of 5B was considered optimum for the effective mitigation of PPV. The effect of the depth of placement of geocell on the PPV is shown in Fig. 5b. Percentage reduction in PPV response was found inversely proportional to the depth of placement of geocell (U) under the concrete block. It demonstrates that the depth of placement of geocell is a crucial factor in reducing the velocity of vibration. For the substantial reduction of PPV, the placement of geocell is suggested at the depth of 0.1B. With the increase in the depth of placement of geocell, there could be a possibility of reflection of induced vibrations.

Table 3 Properties of the geocell reinforcement

| Property type	Parameter	Value
Physical	Polymer composition	NPA
	Cell depth (mm)	120
	Weld spacing (mm)	330
	Thickness of the strip (mm)	1.53
	Cell wall surface	Perforated and textured
	Open area on the surface (%)	16
	Diameter of each hole on the surface (mm)	10
	Total number of cells per square meter	39
	Density (g/cm^3)	0.95 ($\pm$1.5%)
Mechanical	Peak tensile strength (kN/m)	23.8 ($\pm$6%)[a]
	Failure strain (%)	12
	Modulus of elasticity (MPa)	280
Endurance	Coefficient of thermal expansion (ppm/$^\circ$C)	<80
	Durability to UV degradation (minutes)	>400
	Oxidation induction time (minutes)	$\geq$100
	Creep reduction factor	<3.5

[a]ISO 10319 [53]
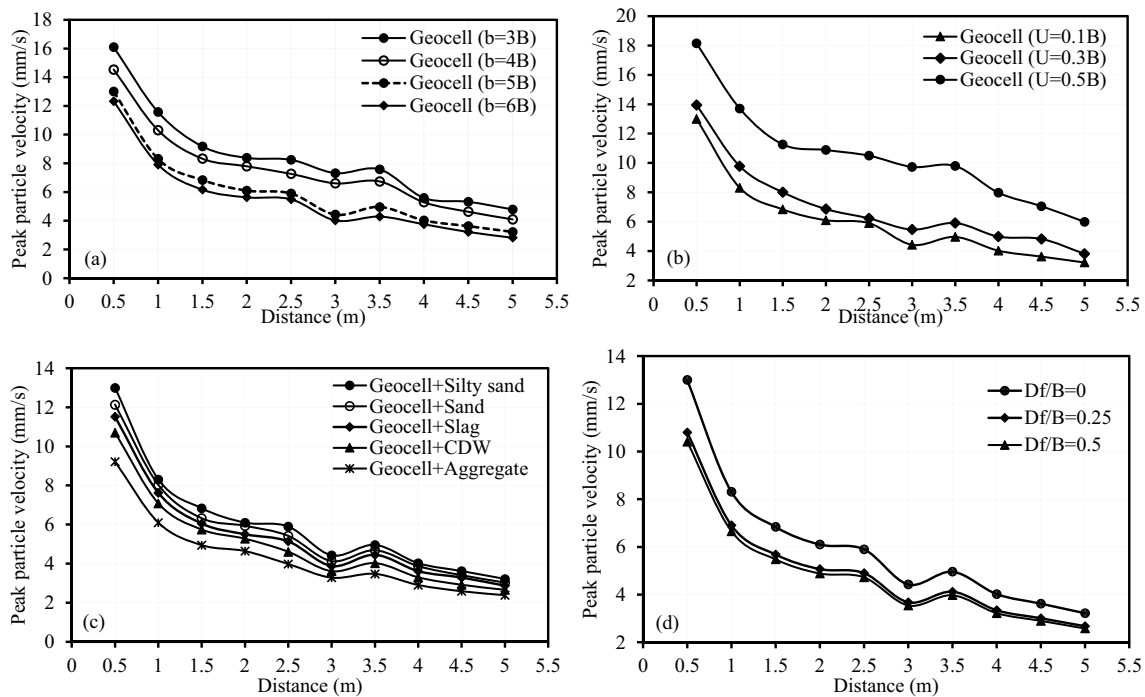
Fig. 5 PPV variation of geocell reinforced bed with **a** width of geocell mattress; **b** depth of placement of geocell; **c** infill material modulus; and **d** embedment of footing

Figure 5c shows the PPV variation with a different modulus of infill material. The geocell pockets were filled with five different materials of varying elastic modulus ranging from 28.3 to 60 MPa. Regardless of distance, PPV values observed in the aggregate infilled case were much lesser than other materials. It reveals that, selecting the infill material with higher modulus results in better mitigation of PPV. The improvement in the damping ratio of the geocell reinforced bed by virtue of the higher elastic modulus of infill material was the reason for the maximum reduction of PPV. Hence, increasing the modulus of infill material is an alternative way of enriching the screening efficacy of geocell reinforced

beds. The effect of footing embedment on PPV in the presence of a geocell reinforced bed is shown in Fig. 5d.

A reduction in PPV values was observed with the increase in footing embedment. Not much variation in PPV was observed beyond the depth of embedment of 0.25B. Hence, minimum D_f is beneficial for a significant reduction of PPV. The reported PPV results for geocell-reinforced cases were corresponding to the dynamic excitation of 1.5 kN. In addition, PPV response for all the cases was also studied at the dynamic force of 1 kN. At a dynamic force of 1 kN, the observed PPV trend was similar to that of 1.5 kN dynamic force with reduced magnitude. Hence, PPV variation corresponding to 1 kN dynamic force has not been presented in the manuscript. However, PPV response corresponding to both the dynamic forces was used to develop the PPV prediction models.

Dataset

Dataset used in the present study comprised of input and output data of parameters. Overall, the total database consists of 240 PPV records collected from the experiment were used to develop the PPV prediction model. In practice, a variation of PPV in the presence of a geocell reinforced bed majorly relies on reinforcement geometry, infill material, footing condition, foundation bed, and vibration source characteristics. It is worth mentioning that the consideration of all the parameters in the model development also brings more uncertainties. In addition, the use of more input parameters may not be able to improve predictive performance. Thus, to select the appropriate number of input parameters trial and error method was carried out using GP. Overall, four different cases with the change in input parameters were considered as per Table 4. The coefficient of determination (R^2) was used to assess the predictive performance of each condition. From the analysis, higher R^2 was observed in case-1 compared to other cases. It reveals that the model

Table 4 Influence of input parameters on the outcome of a model

Condition	Input parameters	Coefficient of correlation (R^2)	
		Training	Testing
Case 1	$X_1, X_2, X_3, X_4, X_5, X_6$	0.9918	0.9825
Case 2	$X_1, X_2, X_3, X_4, X_5, X_6, X_7$	0.9859	0.9779
Case 3	$X_1, X_2, X_3, X_4, X_5, X_6, X_7, X_8$	0.9819	0.9698
Case 4	$X_1, X_2, X_3, X_4, X_5, X_6, X_7, X_8, X_9$	0.985	0.9763

X_1 is the distance from the source in m; X_2 is the width of geocell in m; X_3 is the depth of placement of geocell in m; X_4 is the modulus of infill material in kPa; X_5 is the depth of embedment in m; X_6 is the dynamic force in kN; X_7 is the tensile strength of geocell in kN/m; X_8 is the bulk unit weight of the foundation bed in kN/m³; and X_9 is the aspect ratio (height to pocket diameter of geocell mattress

with six input predictors is more effective to predict the PPV response. Hence, six parameters, namely, distance from the source of vibration (d); width of geocell mattress (b); depth of placement of geocell (U); depth of embedment of footing (D_f); elastic modulus of infill material (E_g); and the dynamic force (F_d) were selected as input indices.

Figure 6 represents the graphical illustration of input parameters. The width and depth of placement of the geocell mattress incorporate the reinforcement effect in the model. To represent the stiffness behavior of infill material, the elastic modulus of infill material was considered. Depth of embedment of block covers the realistic scenario of partial or fully embedment nature of footing. Dynamic force signifies the characteristics of the vibration source including the weight and operating frequency. Distance from the vibration source accounts for the dissipation of PPV caused by the material damping of soil. On the other side, PPV was considered as an output parameter. Table 5 illustrates the statistical limits of the data of different indices considered in the present study. Prior to the model development, total data have been divided into training, testing, and validation as 70%, 20%, and 10%, respectively.

Evaluation of Statistical Performance

Different parameters were evaluated to study the statistical performance of a developed model. It includes MSE (mean square error), RMSE (root mean square error), R (coefficient of correlation), R^2, and NSE (Nash–Sutcliffe model efficiency) coefficient. To obtain the optimum model, it should possess higher values of R, R^2, and NSE. Similarly, lower values of RMSE, and MSE represent better prediction performance. Table 6 summarizes the list of expressions used to determine the aforementioned performance measures.

From Table 6, MSE is the average of the squares of the errors. The error represents the deviation between the estimated and actual values. Generally, MSE values must be close to zero and always non-negative. RMSE is a different mode of representation of MSE. It is the result of the square root of the standard deviation of residuals and MSE. To measure the strength of the relationship between two variables, the correlation coefficient (R) was determined. It generally ranges from − 1 to 1. The value close to 1 specifies a strong positive relationship between the variables. The coefficient of determination (R^2) describes the amount of variance in the dependent variable, which is anticipated from the independent variable. It is usually expressed between 0 and 1. Finally, the Nash–Sutcliffe model efficiency coefficient (NSE) evaluates the relative magnitude of the residual variance compared to the measured variance and varies between -infinity to one [54]. The training and testing dataset were normalized in the range of [0, 1] using the following equation prior to establish the model.
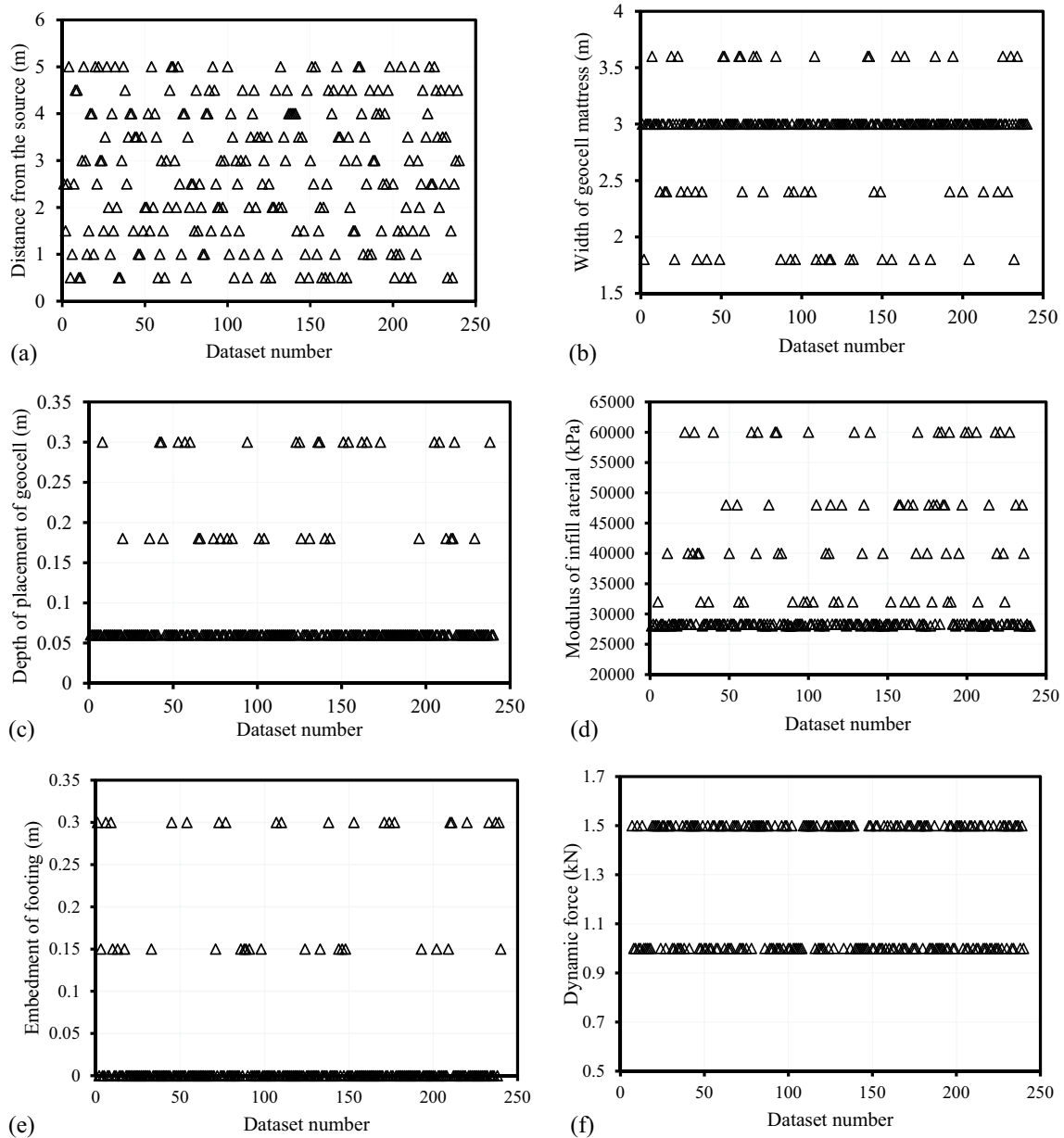
Fig. 6 Input parameter variation with the dataset number: **a** distance from the source; **b** width of geocell mattress; **c** depth of placement of geocell; **d** modulus of infill material; **e** embedment of footing; and **f** dynamic force

Table 5 Summary of the dataset

	X_1 (distance from the source in m)	X_2 (width of geocell in m)	X_3 (depth of placement of geocell in m)	X_4 (elastic modulus of infill material in kPa)	X_5 (depth of embedment in m)	X_6 (dynamic force in kN)	y (PPV in mm/s)
Maximum	5	3.6	0.3	60,000	0.3	1.5	18.146
Minimum	0.5	1.8	0.06	28,300	0	1	2.014
Average	2.75	2.90	0.09	33,816.67	0.04	1.25	5.57
Standard deviation	1.436	0.412	0.071	9910.166	0.089	0.250	2.871

Table 6 Summary of the expressions for different performance indices

Parameter	Expression	Best criteria
MSE (Mean Square Error)	$\frac{1}{N}\sum_{i=1}^{N}(f_i - y_i)^2$	0
RMSE (Root Mean Square Error)	$\sqrt{\frac{1}{N}\sum_{i=1}^{N}(f_i - y_i)^2}$	0
R (Coefficient of Correlation)	$\frac{N(\sum f_i y_i)-(\sum f_i)(\sum y_i)}{\left[\sqrt{N\sum y_i^2-(y_i)^2}\right]\left[\sqrt{N\sum f_i^2-(f_i)^2}\right]}$	1
R^2 (Coefficient of Determination)	$1-\left(\frac{\sum_{i=1}^{N}(f_i-y_i)^2}{\sum_{i=n}^{N}f_i^2}\right)$	1
NSE (Nash–Sutcliffe model efficiency coefficient)	$1-\left[\frac{\sum_{i=1}^{N}(f_i-y_i)^2}{\sum_{i=1}^{N}(y_i-y_{\text{mean}})^2}\right]$	1

N represents total number of observations, f_i and y_i are the experimental and predicted PPV values, respectively

$$y_n = \frac{y - y_{\min}}{y_{\max} - y_{\min}} \qquad (3)$$

where y_n is the normalized value of variable y, $y_{\max}$ and $y_{\min}$ represent the maximum and minimum values of the variable y, respectively. Finally, obtained PPV was denormalized using the following expression.

$$y = (y_n)(y_{\max} - y_{\min}) + y_{\min} \qquad (4)$$

Development of PPV Prediction Model

Prediction Model Using GP

In the case of MGGP, parameters used for finding the best symbolic expressions are the population size, number of generations, number of genes, tournament size, Elite fraction, Mutation-Crossover-Copy fractions, gene depth, and Build method. The best value of each parameter was obtained by running the model numerous times with distinct combinations of parameters. The optimal values of various controlling parameters were determined from the trial and error method listed in Table 7. During the trial and error process, a specific parameter was varied for a range by keeping the remaining parameters constant.

This process was continued until achieving the optimal solution. The exercises were carried out three times for eliminating the biases from each solution. Further, the simplified equation resulting from GP to quantify the PPV is expressed by,

Table 7 Optimum details of control parameters for GP

S. No	Controlling parameter	Optimum value	Range
1	Build method	Ramped half and half	Full-Grow-Ramped half and half
2	Max gene depth	6	2–10
3	Max genes	10	1–12
4	M-C-D probabilities	0.6–0.35–0.05	0–1
5	Tournament size (%)	60	10–80
6	Elite fraction	0.5	0.05–0.5
7	Population	1000	25–1500
8	Generation	100	10–150

$$
\begin{aligned}
y = {}& 1.22\sin^2(x_2) - 465.0\cos\left(x_3^2 \times x_6^2\right) \\
& - 0.385\sin\left(x_1^8\right) + 5.84\sin\left(\frac{x_6(x_3 - x_5)}{\sqrt{x_1}}\right) \\
& + 59.2\sin\left(x_1\cos\left(x_3^2\right)\right) + 0.144\exp\left(\cos\left(x_4^2\right)\right) \\
& + 918.0\sqrt{\frac{x_6\sqrt{x_6}}{x_1 x_4}} - 60.2\sin(x_1) \\
& + 0.00361\cos(\sin x_2)\exp\left(\frac{x_5}{x_3}\right) \\
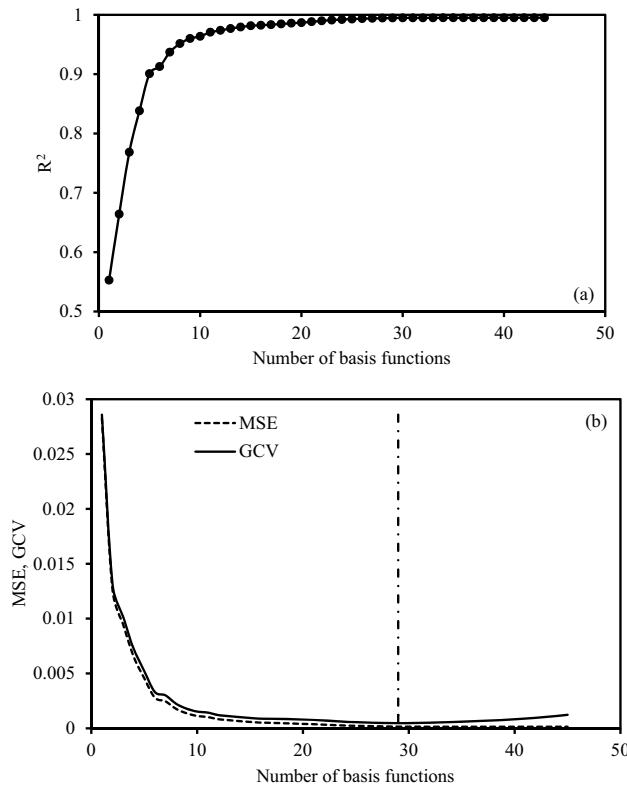& - 0.144x_1^2 + \frac{(2.07\sin(x_2))^2}{\sqrt{x_1}} + 467.0
\end{aligned}
$$

$$\hspace{10cm}(5)$$

Fig. 7 Variation of predictors with the number of basis functions: **a** R^2; and **b** MSE and GCV

where x_1 is the distance from the source in m; x_2 is the width of geocell in m; x_3 is the depth of placement of geocell in m; x_4 is the modulus of infill material in kPa; x_5 is the depth of embedment in m; x_6 is the dynamic force in kN; and y is the peak particle velocity in mm/s.

Prediction Model Using MARS

The MATLAB code based on MARS methodology has been used to predict the PPV [55]. It is capable of building the optimum model through the change in the number of basis functions. In the present study, the optimum number of BFs was identified through different performance metrics namely, R^2, MSE, and GCV. The variation of these predictors with the number of BFs is shown in Fig. 7. The R^2 variation was found constant with the increase in BFs beyond 28 (Fig. 7a). Similarly, minimum GCV was observed when the number of BFs was equal to 28. Increase in the number of BFs beyond 28 increased the GCV as shown in Fig. 7b. It reveals the overfitting among the predicted functions. Thus, 28 numbers of BFs were selected to develop the model. The expression corresponding to each BF is summarized in Table 8.

Table 8 Summary of expressions for basis functions

BF number	Expression
1	$BF1 = \max(0, x_1 - 0.22)$
2	$BF2 = \max(0, 0.22 - x_1)$
3	$BF3 = \max(0, x_3 - 0.5)$
4	$BF4 = \max(0, 0.5 - x_3)$
5	$BF5 = \max(0, x_2 - 0.66)$
6	$BF6 = \max(0, 0.66 - x_2)$
7	$BF7 = \max(0, x_4 - 0.009374)$
8	$BF8 = \max(0, 0.0093749 - x_4)$
9	$BF9 = \max(0, x_1 - 0.11)$
10	$BF10 = \max(0, 1 - x_6) \times \max(0, x_1 - 0.22)$
11	$BF11 = \max(0, 1 - x_6) \times \max(0, 0.22 - x_1)$
12	$BF12 = BF9 \times \max(0, x_4 - 0.0093749)$
13	$BF13 = BF9 \times \max(0, 0.0093749 - x_4)$
14	$BF14 = \max(0, 1 - x_6) \times \max(0, x_4 + 0)$
15	$BF15 = \max(0, 1 - x_6) \times \max(0, 0.66 - x_2)$
16	$BF16 = BF3 \times \max(0, x_1 - 0.11)$
17	$BF17 = BF9 \times \max(0, 0.33 - x_2)$
18	$BF18 = BF1 \times \max(0, 0.0093749 - x_4)$
19	$BF19 = \max(0, 1 - x_6) \times \max(0, x_4 - 0.125)$
20	$BF20 = BF4 \times \max(0, 1 - x_6)$
21	$BF21 = \max(0, 1 - x_6) \times \max(0, 1 - x_5)$
22	$BF22 = BF1 \times \max(0, 0.33 - x_2)$
23	$BF23 = BF6 \times \max(0, x_1 - 0.66)$
24	$BF24 = BF6 \times \max(0, x_1 - 0.77)$
25	$BF25 = BF4 \times \max(0, 0.55 - x_1)$
26	$BF26 = BF4 \times \max(0, x_1 - 0.66)$
27	$BF27 = BF4 \times \max(0, x_1 - 0.44)$
28	$BF28 = BF4 \times \max(0, 0.44 - x_1)$

Finally, the PPV prediction equation (y) obtained from the MARS method is expressed as,

$$
\begin{aligned}
y = {} & 0.2215 - 1.5468 \times BF1 + 2.2992 \times BF2 \\
& + 0.4959 \times BF3 - 0.2821 \times BF4 \\
& - 0.08549 \times BF5 + 0.3225 \times BF6 \\
& - 0.1158 \times BF7 - 11.2947 \times BF8 + 1.2386 \times BF9 \\
& + 0.05819 \times BF10 - 0.3597 \times BF11 + 0.05691 \times BF12 \\
& + 40.6836 \times BF13 - 0.1616 \times BF14 - 0.0791 \times BF15 \\
& - 0.1795 \times BF16 - 2.1748 \times BF17 - 37.0667 \times BF18 \\
& + 0.0529 \times BF19 - 0.1324 \times BF20 - 0.02376 \times BF21 \\
& + 2.4643 \times BF22 - 1.1572 \times BF23 + 1.1676 \times BF24 \\
& + 1.4031 \times BF25 - 0.7548 \times BF26 + 0.7782 \times BF27 \\
& - 1.5092 \times BF28
\end{aligned}
$$

$$(6)$$

Fig. 8 Predicted PPV versus observed PPV of training data using: **a** GP; and **b** MARS model
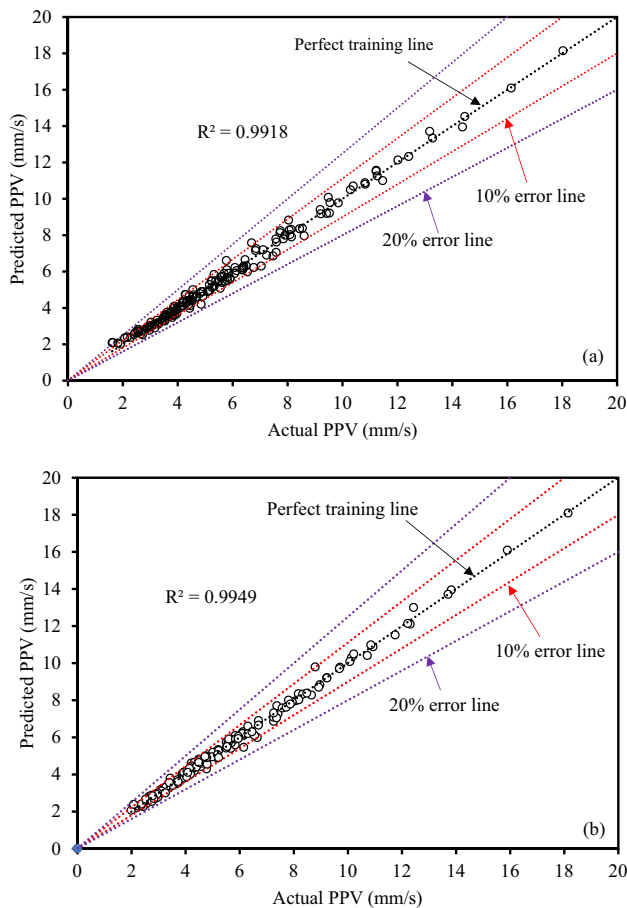

Fig. 9 Predicted PPV versus observed PPV of testing data using: **a** GP; and **b** MARS model

Performance of Developed Models

Figure 8a, b shows the goodness of fit between predicted and actual values of PPV for the training dataset obtained from both models. To understand the accuracy of each model, the value of the coefficient of determination (R^2) has been presented. From figure, a good match was noticed between predicted and observed PPV values. Similarly, Fig. 9a, b shows the correlation between predicted and actual PPV values for the testing dataset. Regardless of the dataset, the MARS model has exhibited a higher R^2 value in comparison with the GP model. For further comparison, ± 10%, and ± 20% error lines have been drawn in the figures. It was noticed that the maximum PPV outputs produced from the MARS model fall between the ± 10% error lines in both the training and testing conditions as compared to the GP model. It reveals that the MARS model could predict the PPV response with a less than 10% error. For further quantifying the predictive performance of each model, different statistical parameters for the training,
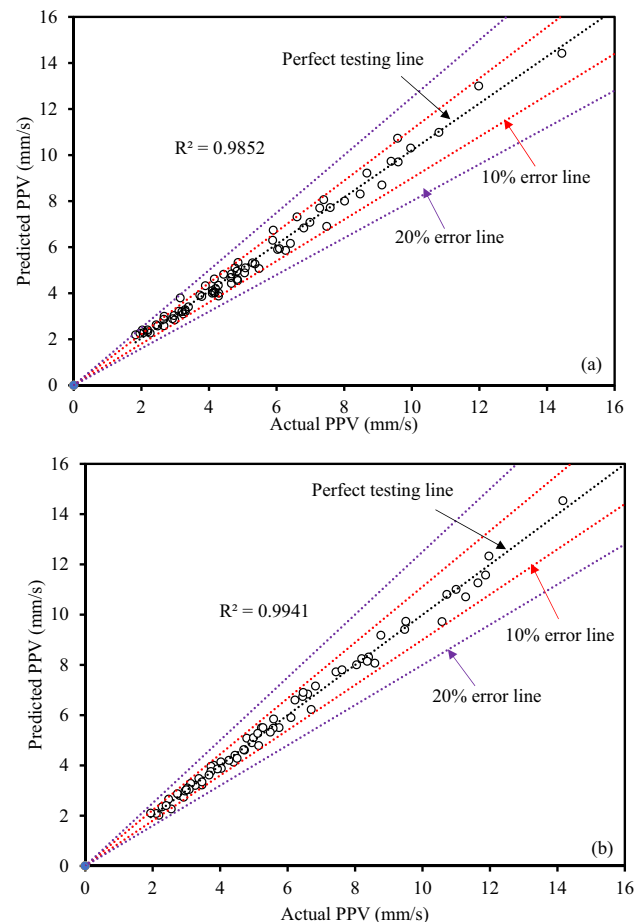
validation, and testing datasets were calculated and listed in Table 9. It was observed that the MARS model has exhibited the minimum values of MSE and RMSE, and higher values of r, R^2, and NSE. It indicates the effective training and testing ability of the MARS model in comparison to the GP model.

Sensitivity Analysis

Sensitivity analysis was performed to understand the influence of each input parameter on the PPV response. It is advantageous to examine the parameter, which significantly influences the outcome of a model. Overall, a sensitivity study is useful to minimize the number of input parameters and to reduce the iterations count required to run the model without jeopardizing the result. Generally, the approach followed for conducting the sensitivity analysis is different for different models.

In GP, the sensitivity analysis is performed by determining the frequency of each input parameter. Several researchers have followed a similar method [56, 57]. The frequency

Table 9 Summary of statistical parameters for different models

Statistical parameter	GP			MARS		
	Training	Validation	Testing	Training	Validation	Testing
MSE	0.073	0.079	0.1154	0.0402	0.0366	0.0605
RMSE	0.2703	0.2811	0.3397	0.2005	0.1913	0.2469
r	0.996	0.9958	0.992	0.9975	0.9981	0.9953
R^2	0.992	0.9918	0.984	0.9949	0.9964	0.9906
NSE	0.992	0.99	0.983	0.995	0.996	0.994
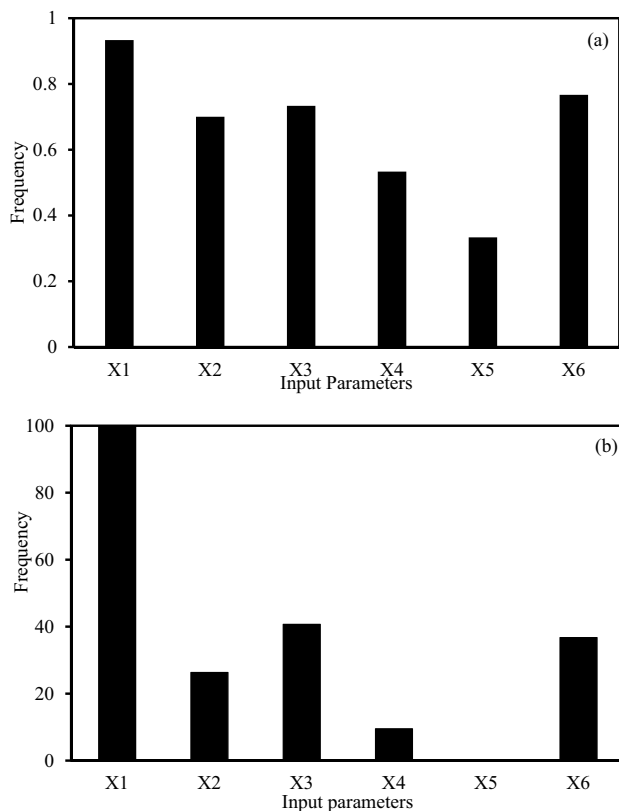
Fig. 10 Frequency variation of different input parameters using **a** GP; and **b** MARS model

Fig. 11 Percentage change in PPV with the percentage variation of input parameters: **a** GP; and **b** MARS model

was evaluated based on the appearance of a variable in the best thirty programs developed through MGGP. It is generally represented between 0 to 1. The value 1 indicates a 100% appearance of a parameter in all the evolved programs. Variation of frequency for different input parameters is shown in Fig. 10a. Interestingly, the sensitivity results of MGGP were also revealed that distance from vibration source to point of measurement is the most influencing parameter. In reality, distance from the vibration source highlights the damping behavior of soil mass. A similar observation was also noticed from the MARS model as shown in Fig. 10b. The input parameter, which exhibits a high amount of variance, is considered as the most influencing parameter in the MARS. It is worth mentioning that, this observation is true from the
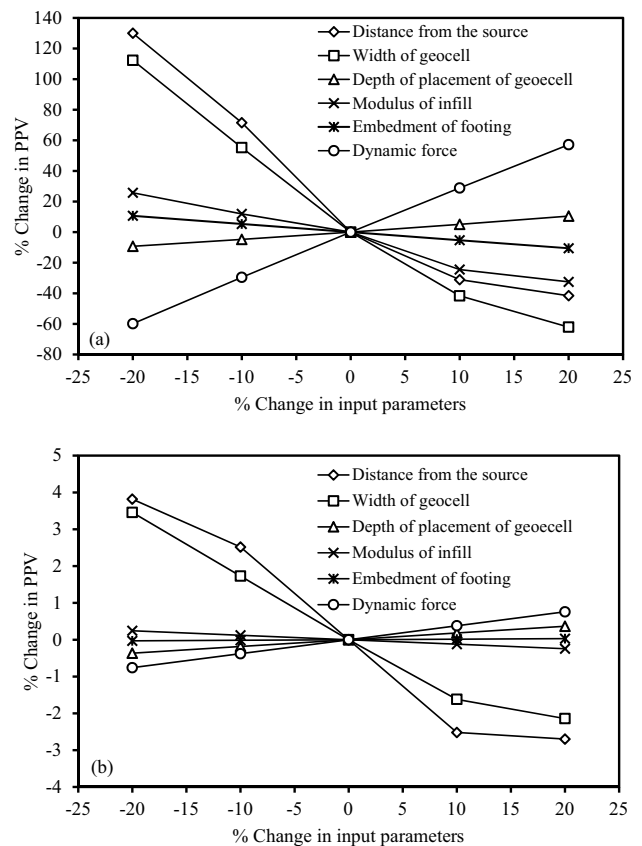
practical point of view as well. Higher dissipation of vibration energy with the increase in distance by soil damping is the reason for the reduction of PPV.

Further, the influence of each input parameter on the PPV was also studied. All the input parameters were varied between − 20% and 20% of the mean value. Figure 11 shows the variation of PPV with the percentage change of input parameters for different models. Distance from vibration source to point of measurement was found as the most influencing parameter in the case of both models. Slight variation in distance resulted in a significant variation of PPV. Apart from distance, the trend of other parameters namely, width of geocell, modulus of infill, and embedment of footing was
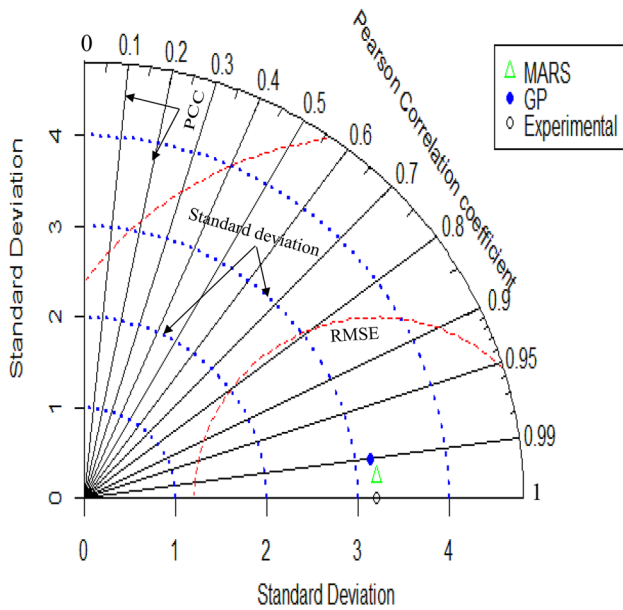
Fig. 12 Performance comparison between the predicted and experimental response using Taylor's diagram

Fig. 13 Comparison of model performance with the field test results for **a** case (i); and **b** case (ii)

observed similar to field study. It highlights the better generalization ability of GP and MARS models in anticipating the response of each input predictor.

Finally, Taylor's diagram is presented in Fig. 12 to understand the overall predictive performance of both models. Generally, this diagram visualizes, how close the developed models can predict the experimental PPV response in a single framework. In the figure, black solid lines indicate the Pearson correlation coefficient (PCC). Similarly, dotted radial lines shown with the blue and red color represent the standard deviation (SD), and RMSE, respectively. For the experimental database, SD and PCC values were observed as 3.23 and 1, respectively. The SD and PCC values of (3.21, 0.995), and (3.11, 0.989) were observed for MARS, and GP models, respectively. Thus, this observation reveals that the performance of the MARS model is much closer to the experimental response than the GP model. Thus, it is admissible that the developed MARS model is more reliable in predicting the PPV response than GP.

Experimental Versus Model Performance

Apart from the series of vibration tests described in the experimental study, two more field tests were conducted to assess the performance of developed models. Though the differences in mechanisms and performance of the selected methods, this comparison is useful in assessing the best-suited method for predicting the PPV at the unknown loading conditions. Practically,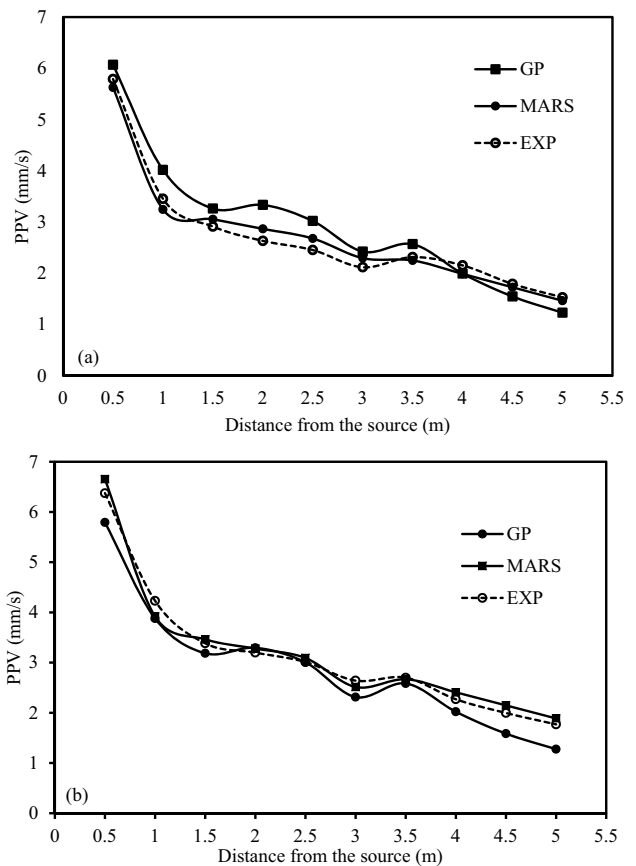 footings supporting the vibration sources are subjected to different dynamic loading conditions. This analysis is intended to highlight the efficacy of the proposed model in predicting the PPV response at the involvement of different dynamic loads. The following are the details of conducted field tests with varying configurations of input parameters.

Case (i): $F_d = 0.5$ kN; $U = 0.1B$; $D_f = 0.25B$; $b = 5B$; and silty sand infill material.

Case (ii): $F_d = 0.5$ kN; $U = 0.1B$; $D_f = 0B$; $b = 5B$; and CDW infill material.

The dynamic force considered in the above-mentioned cases was not in the part of a dataset used to develop the prediction model. A comparison of field test results with the model results for the two different cases is shown in Fig. 13a, b. Irrespective of the distance, the percentage deviation between the experimental and predicted PPV was observed less in the case of MARS as compared to the GP model.

For the precise computation of error variation at each distance, the parameter absolute error was calculated. It is determined by,
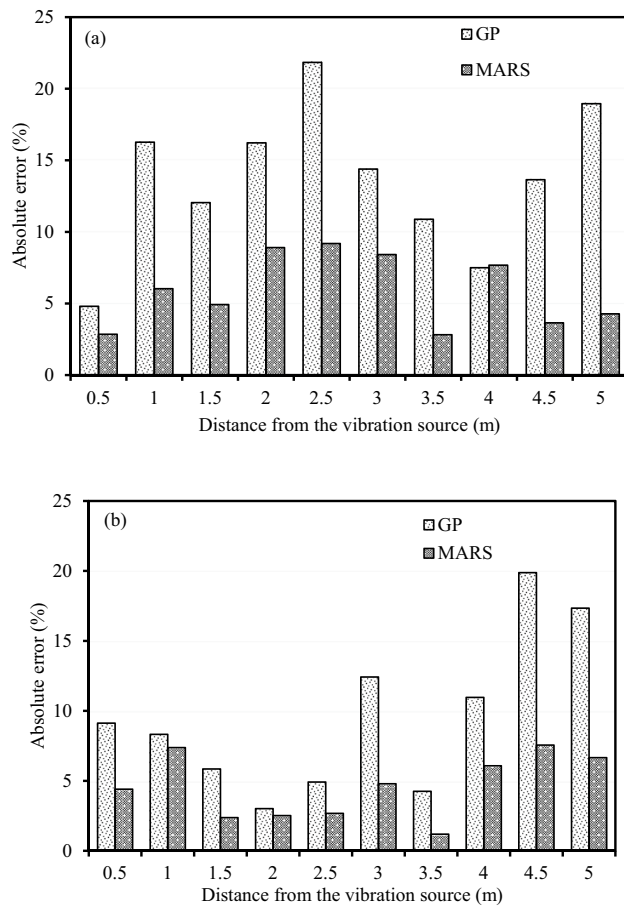
Fig. 14 Absolute error variation with the distance for **a** case (i); and **b** case (ii)

$$\text{Absolute error (\%)} = \frac{|\text{Experimental PPV} - \text{Predicted PPV}|}{\text{Experimental PPV}} \times 100$$

The absolute error variation at each distance for both the cases is shown in Fig. 14. Even for the unknown dataset, less than 10% absolute error was observed in the case of the MARS model for both cases. Whereas, a higher error was noticed in the case of the GP model as compared to the MARS model. It might be attributed due to the computational efficiency of the MARS model in terms of building the flexible models, stepwise searching, and quantifying the contribution of the individual input parameter [58].

Conclusions

In the present study, GP, and MARS models were established to predict the PPV response of the soil beds reinforced with geocell reinforcement. The data set of 240 PPV records obtained from the field vibration tests were used to develop the models. The salient points drawn from the present study are:

1. As per the parametric investigation, the consideration of six input parameters was found effective to develop the PPV prediction model for achieving better performance and avoiding the complexity of a model.
2. Upon the model development, different metrics namely, coefficient of determination, mean square error, root mean square error, and the Nash–Sutcliffe model efficiency coefficient were evaluated to understand the prediction performance. The values of the aforesaid matrices endorsed the excellent performance of the developed models. Particularly, the MARS model has displayed a higher R^2 value compared to the GP model in training, validation, and testing phases.
3. Sensitivity analysis of both the models revealed that the parameter representing the distance from the vibration source to the point of measurement (i.e. damping) influences the PPV most. Further, the decreasing order of the importance of other parameters followed as, the depth of placement of geocell, dynamic force, the width of geocell, and modulus of infill material.
4. The MARS model was found efficient to predict the PPV response with less than 10% error as compared to the GP model.
5. Based on Taylor's diagram, the performance of the MARS model was found superior over the GP model in predicting the experimental response. Thus, it is recommended for predicting the PPV response of geocell reinforced foundation beds.

Overall, this study is an initiative for predicting the PPV variation of a geocell-reinforced bed subjected to vibration loading. The present model applies to specific soil types and loading conditions. Due to the tedious nature of field experiments, the density of the foundation bed, geocell tensile strength, and aspect ratio (height to pocket diameter) were maintained constant in the present study. Using the principles highlighted in the present study, the prediction equations could be modified for other soil types and loading stipulations.

References

1. American Association of State Highway and Transportation Officials (AASHTO) (1990) Standard Recommended Practice for Evaluation of Transportation-related Earth borne Vibrations. Washington, DC

2. Standard B (1993) BS7385-2 Evaluation and measurement for vibration in buildings. In: Guide to damage levels from ground-borne vibration

3. Dhar BB, Pal RP, Singh RB (1993) Optimum blasting for Indian geo-mining conditions suggestive standard and guidelines. CMRI Publication, India

4. Building and Civil Engineering Standards Committee (1999) DIN4150-3 structural vibration part 3: effects of vibration on structures. DIN Germany Institute, Germany

5. Directorate General of Mines & Safety (DGMS, India) (1997) Technical Circular 7 of 1997, India, p 6

6. Standard S (1978) SN 640 312: effects of vibration of construction. In: Swiss Association of Standarization, Zurich

7. Johnson AP, Hannen WR (2015) Vibration limits for historic buildings and art collections. APT Bull J Preserv Technol 46(2/3):66–74

8. Singh PK, Roy MP (2010) Damage to surface structures due to blast vibration. Int J Rock Mech Min Sci 47(6):949–961

9. Tafreshi SM, Zarei SE, Soltanpour Y (2008) Cyclic loading on foundation to evaluate the coefficient of elastic uniform compression of sand. In: The 14th world conference on earthquake engineering, Beijing, China

10. Hegde A, Sitharam TG (2016) Behaviour of geocell reinforced soft clay bed subjected to incremental cyclic loading. Geomech Eng 10(4):405–422

11. Hegde A (2017) Geocell reinforced foundation beds-past findings, present trends and future prospects: a state-of-the-art review. Constr Build Mater 154:658–674

12. Venkateswarlu H, Ujjawal KN, Hegde A (2018) Laboratory and numerical investigation of machine foundations reinforced with geogrids and geocells. Geotext Geomembr 46(6):882–896

13. Ujjawal KN, Venkateswarlu H, Hegde A (2019) Vibration isolation using 3D cellular confinement system: a numerical investigation. Soil Dyn Earthq Eng 119:220–234

14. Samui P, Sitharam TG, Kurup PU (2008) OCR prediction using support vector machine based on piezocone data. J Geotech GeoEnviron Eng 134(6):894–898

15. Cabalar AF, Cevik A, Gokceoglu C (2012) Some applications of adaptive neuro-fuzzy inference system (ANFIS) in geotechnical engineering. Comput Geotech 40:14–33

16. Sethy BP, Patra CR, Sivakugan N, Das BM (2017) Application of ANN and ANFIS for predicting the ultimate bearing capacity of eccentrically loaded rectangular foundations. Int J Geosynth Ground Eng 3(4):1–14

17. Suthar M, Aggarwal P (2018) Predicting CBR value of stabilized pond ash with lime and lime sludge using ANN and MR models. Int J Geosynth Ground Eng 4(1):1–7

18. Sahu R, Patra CR, Sivakugan N, Das BM (2017) Use of ANN and neuro fuzzy model to predict bearing capacity factor of strip footing resting on reinforced sand and subjected to inclined loading. Int J Geosynth Ground Eng 3(3):1–15

19. Raja MNA, Shukla SK, Khan MUA (2021) An intelligent approach for predicting the strength of geosynthetic-reinforced subgrade soil. Int J Pavement Eng 2021:1–17

20. Dal K, Cansiz OF, Ornek M, Turedi Y (2019) Prediction of footing settlements with geogrid reinforcement and eccentricity. Geosynth Int 26(3):297–308

21. Raja MNA, Shukla SK (2020) An extreme learning machine model for geosynthetic-reinforced sandy soil foundations. Proce Inst Civ Eng Geotech Eng 2020:1–21

22. Raja MNA, Shukla SK (2021) Predicting the settlement of geosynthetic-reinforced soil foundations using evolutionary artificial intelligence technique. Geotext Geomembr. https://doi.org/10.1016/j.geotexmem.2021.04.007

23. Raja MNA, Shukla SK (2021) Multivariate adaptive regression splines model for reinforced soil foundations. Geosynth Int 2021:1–23

24. Iphar M, Yavuz M, Ak H (2008) Prediction of ground vibrations resulting from the blasting operations in an open-pit mine by adaptive neuro-fuzzy inference system. Environ Geol 56(1):97–107

25. Khandelwal M, Singh TN (2009) Prediction of blast-induced ground vibration using artificial neural network. Int J Rock Mech Min Sci 46(7):1214–1222

26. Monjezi M, Ghafurikalajahi M, Bahrami A (2011) Prediction of blast-induced ground vibration using artificial neural networks. Tunn Undergr Space Technol 26(1):46–50

27. Amnieh HB, Siamaki A, Soltani S (2012) Design of blasting pattern in proportion to the peak particle velocity (PPV): Artificial neural networks approach. Saf Sci 50(9):1913–1916

28. Ghoraba S, Monjezi M, Talebi N, Armaghani DJ, Moghaddam MR (2016) Estimation of ground vibration produced by blasting operations through intelligent and empirical models. Environ Earth Sci 75(15):1137

29. Muduli PK, Das SK (2014) Evaluation of liquefaction potential of soil based on standard penetration test using multi-gene genetic programming model. Acta Geophys 62(3):529–543

30. Mohammadzadeh D, Bazaz JB, Yazd SVJ, Alavi AH (2016) Deriving an intelligent model for soil compression index utilizing multi-gene genetic programming. Environ Earth Sci 75(3):262

31. Zhou J, Bejarbaneh BY, Armaghani DJ, Tahir MM (2019) Forecasting of TBM advance rate in hard rock condition based on artificial neural network and genetic programming techniques. Bull Eng Geol Env 2019:1–16

32. Sharma S, Venkateswarlu H, Hegde A (2019) Application of machine learning techniques for predicting the dynamic response of geogrid reinforced foundation beds. Geotech Geol Eng 37(6):4845–4864

33. Attoh-Okine NO, Cooger K, Mensah S (2009) Multivariate adaptive regression (MARS) and hinged hyperplanes (HHP) for doweled pavement performance modeling. Constr Build Mater 23(9):3020–3023

34. Samui P, Kurup P (2012) Multivariate adaptive regression spline and least square support vector machine for prediction of undrained shear strength of clay. Int J Appl Metaheuristic Comput 3(2):33–42

35. Lashkari A (2013) Prediction of the shaft resistance of non-displacement piles in sand. Int J Numer Anal Meth Geomech 37(8):904–931

36. Zhang W, Goh AT, Zhang Y, Chen Y, Xiao Y (2015) Assessment of soil liquefaction based on capacity energy concept and multivariate adaptive regression splines. Eng Geol 188:29–37

37. Goh AT, Zhang Y, Zhang R, Zhang W, Xiao Y (2017) Evaluating stability of underground entry-type excavations using multivariate adaptive regression splines and logistic regression. Tunn Undergr Space Technol 70:148–154

38. Ganesh R, Khuntia S (2018) Estimation of pullout capacity of vertical plate anchors in cohesionless soil using MARS. Geotech Geol Eng 36(1):223–233

39. Pattanaik ML, Choudhary R, Kumar B (2019) Prediction of frictional characteristics of bituminous mixes using group method of data handling and multigene symbolic genetic programming. Eng Comput 2019:1–14

40. Arthur CK, Temeng VA, Ziggah YY (2019) Multivariate adaptive regression splines (MARS) approach to blast-induced ground vibration prediction. Int J Min Reclam Env 2019:1–25

41. Hosseini SA, Tavana A, Abdolahi SM, Darvishmaslak S (2019) Prediction of blast induced ground vibrations in quarry sites: a comparison of GP, RSM and MARS. Soil Dyn Earthq Eng 119:118–129

42. Koza JR (1994) Genetic programming as a means for programming computers by natural selection. Stat Comput 4(2):87–112

43. Alavi AH, Aminian P, Gandomi AH, Esmaeili MA (2011) Genetic-based modeling of uplift capacity of suction caissons. Expert Syst Appl 38(10):12608–12618

44. Searson DP, Leahy DE and Willis MJ (2010) GPTIPS: an open source genetic programming toolbox for multigene symbolic regression. In:Proceedings of the International multiconference of engineers and computer scientists (Vol 1, pp 77–80). Hong Kong: IMECS

45. Searson DP (2015) GPTIPS 2: an open-source software platform for symbolic data mining. In:Handbook of genetic programming applications (pp 551–573). Springer, Cham

46. Zhang WG, Goh ATC (2013) Multivariate adaptive regression splines for analysis of geotechnical engineering systems. Comput Geotech 48:82–95

47. Craven P, Wahba G (1979) Estimating the correct degree of smoothing by the method of generalized cross-validation. Numer Math 31:377–403

48. Venkateswarlu H, Hegde A (2020) Effect of influencing parameters on the vibration isolation efficacy of geocell reinforced soil beds. Int J Geosyn Ground Eng 6:1–17

49. ASTM D-4253 (2016) Standard test methods for maximum index density and unit weight of soils using a vibratory table. In: ASTM International, West Conshohocken, PA, USA

50. ASTM D-4254 (2016) Standard test methods for minimum index density and unit weight of soils using a vibratory table. In: ASTM International, West Conshohocken, PA, USA

51. ASTM D-4767 (2011) Standard test method for consolidated undrained triaxial compression test for cohesive soils. In: ASTM International, West Conshohocken, PA, USA

52. ASTM D-3080 (1998) Standard test method for direct shear test of soils under consolidated drained conditions. In: ASTM International, West Conshohocken, PA, USA

53. ISO, E. 10319 (2015) Geotextiles, wide width tensile test. In: Comité Européen de Normalisation, Brussels

54. Nash JE, Sutcliffe JV (1970) River flow forecasting through conceptual models part I—a discussion of principles. J Hydrol 10(3):282–290

55. Math Works (2001) Matlab user's manual. Version 2017b, The MathWorks, Inc., Natick

56. Garson GD (1991) Interpreting neural-network connection weights. AI Expert 6(4):46–51

57. Mohammadzadeh D, Bazaz JB, Alavi AH (2014) An evolutionary computational approach for formulation of compression index of fine-grained soils. Eng Appl Artif Intell 33:58–68

58. Goh ATC, Zhang W, Zhang Y, Xiao Y, Xiang Y (2018) Determination of earth pressure balance tunnel-related maximum surface settlement: a multivariate adaptive regression splines approach. Bull Eng Geol Env 77(2):489–500